Structure of water under subcritical and supercritical conditions studied by solution X-ray diffraction

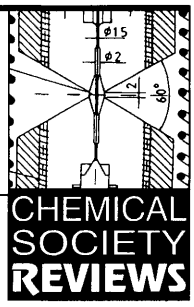

Hitoshi Ohtaki,[a] Tamás Radnai[b] and Toshio Yamaguchi[c]

[a] *Department of Chemistry, Faculty of Science and Engineering, Ritsumeikan University, 1-1-1 Noji-Higashi, Kusatsu 525-77, Japan*; E-mail: ohtaki@bkc.ritsumei.ac.jp
[b] *Central Research Institute for Chemistry, Hungarian Academy of Sciences, Budapest, P.O. Box 17, H-1525 Hungary;* E-mail: radnait@cric.chemres.hu
[c] *Department of Chemistry, Faculty of Science, Fukuoka University, 8-19-1, Nanakuma, Jonan-ku, Fukuoka 814-80, Japan;* E-mail: yamaguch@sunsp1.sc.fukuoka-u.ac.jp

Structures of water and aqueous electrolyte solutions under sub- and super-critical conditions studied mainly by X-ray diffraction and also by neutron diffraction are reviewed and the experimental results are compared with those reported by using computer simulations. Some Raman spectroscopic data are included for discussing the existence of hydrogen bonds in water at high temperature and high pressures (HTHPs).

The authors propose a classification of supercritical water into three categories: (*a*) low density water, (*b*) medium density water, and (*c*) high density water, because density is a very important thermodynamic quantity to describe properties of sub- and super-critical water.

From changes in the water–water intermolecular distance and the coordination number of water with temperature and pressure, and especially with density at HTHP, the authors conclude that the compact tetrahedral-like water structure is decomposed and long-distance water–water interactions increase with temperature and pressure, and they propose a model for water: under supercritical conditions water consists of small clusters, much smaller aggregates such as oligomers, and even monomeric gas-like water molecules.

1 Introduction

The structural chemistry of water has not yet been fully established even under normal conditions despite a long history of investigation after the pioneering work on solution X-ray diffraction in 1930–1931 and the first model of water's structure by Bernal and Fowler[1] in 1933 on the basis of X-ray diffraction

Hitoshi Ohtaki graduated from Nagoya University in 1955 and obtained MSc and DrSc degrees in 1957 and 1961, respectively, from Nagoya University. He became a research associate of the Tokyo Institute of Technology in 1959. He studied complex equilibria under the supervision of Prof. L. G. Sillén, Stockholm, Sweden, as a postdoctoral research fellow from 1961 to 1964. He was appointed Lecturer of Nagoya University in 1965 and promoted to Associate Professor in 1967. In 1970 he moved back to Tokyo Institute of Technology as an Associate Professor, and then became a Full Professor in 1973. As Professor of the Institute for Molecular Science of the Okazaki National Research Institutes from 1988, he was the Director of the Coordination Chemistry Laboratories. On retirement in 1993 he became Professor Emeritus of Tokyo Institute of Technology and the Graduate University for Advanced Studies. He was appointed as Professor of Ritsumeikan University in 1993 and the Director of the Institute of Science and Engineering of Ritsumeikan University in 1994. He has published more than 200 research papers and reviews, and several books.

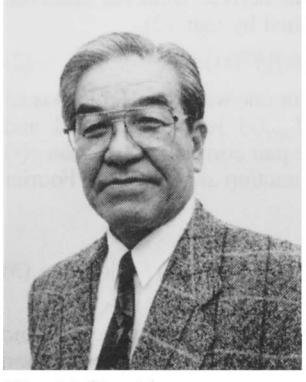

Hitoshi Ohtaki

Tamás Radnai finished his university course in the Eötvös Loránd University, Budapest, in 1973 with a degree equivalent to an MSc. He received the Doctor University degree (corresponding to a PhD) from the Eötvös Loránd University in 1977 and the academic title 'Candidate for Chemical Science', a post-PhD degree, in 1991. He served as a research associate with the Ministry of Education, Science and Culture of Japan from 1987 to 1989 and was invited to the Institute for Molecular Science as a Guest Foreign Associate Professor in 1991. He has worked as a member of several international research groups in Italy and Germany. He is a senior fellow of the department of solution chemistry in the Central Research Institute for Chemistry of the Hungarian Academy of Sciences. His main interest includes structural studies of electrolyte solutions by using diffraction methods, as well as computer simulations. He has published more than 60 research papers.

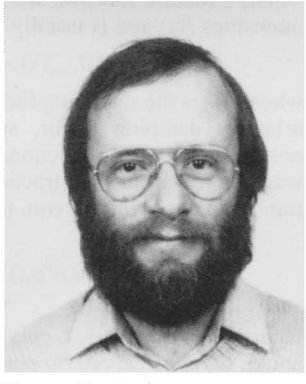

Tamas Radnai

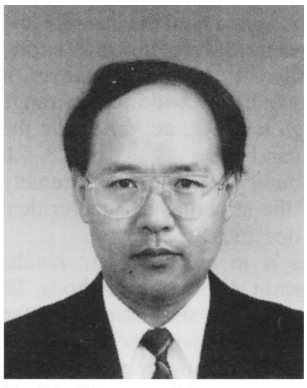

Toshio Yamaguchi

Toshio Yamaguchi graduated from Nagoya Institute of Technology in 1973, and received his PhD degree from Tokyo Institute of Technology in 1978. After terms as a postdoctoral fellow at Gothenburg University, Sweden, from 1979 to 1982 and a research associate at Tokyo Institute of Technology from 1982 to 1986, he was appointed Associate Professor of Fukuoka University in 1986, and then promoted to a Full Professor in 1994. He has published more than 100 research papers.

experiments, not to speak of the study of water's structure at high temperatures and high pressures.

A large amount of thermodynamic data for HTHP and supercritical water has been accumulated in recent years. However, the structures of even simple molecular liquids without extended hydrogen-bonded networks have not been well elucidated under non-ambient conditions. Water, of course, always attracts the interest of many scientists, but due to experimental difficulties, microscopic structural investigations of water at HTHPs and under supercritical conditions have been rare until recently. Spectroscopic investigations have been performed to discuss the structure of subcritical and supercritical water on the basis of changes in vibrational and rotational energies of water molecules.[2–6] However, results obtained on the structure are still limited to discussing hydrogen bonding in supercritical water. The application of computer simulation techniques such as Monte Carlo and molecular dynamics simulations has contributed to a better understanding of water's structure at the molecular level under ambient conditions and at HTHP.

Several attempts have been made to study water in the subcritical and supercritical regions by using computer simulation techniques,[7–14] but it is obvious that the reliability of the simulations can only be confirmed when the simulation data are compared with experiments. Recent technical developments for X-ray and neutron diffraction methods allow us to study the structure of water at HTHPs and even under supercritical conditions. Interest in the use of supercritical water has increased rapidly in recent years, because of the ability of supercritical water to decompose some organic waste. Geochemistry related to subterranean water and hydrothermal synthetic chemistry require a knowledge of HTHP solution chemistry. However, only a limited number of X-ray[15–18] and neutron[19–21] diffraction studies at HTHP have so far been carried out. Nevertheless, we believe that it is worth reviewing recent results on the structure of HTHP water.

The properties of supercritical water are often summarized as follows: (1) the relative permittivity (ε) and viscosity (η) of water steeply decrease around the critical point, (2) the density of supercritical water at the critical point is about 1/3 of that of ambient water, (3) the solubility of ionic and polar substances sharply decreases in supercritical water, (4) on the other hand, the solubility of non-polar substances sharply increases in supercritical water, (5) ionic hydration markedly decreases in supercritical water.

Some properties like (1) and (2) can be explained in terms of hydrogen-bond breaking of the bulk water at HTHP. However, items (3)–(5) may not always be representative of the characteristic properties of supercritical water near the critical point where the density of water is so small that it is *ca.* 1/3 of that of normal water. In such low-density water, the solubility of ionic and polar substances may be decreased due to the lack of water molecules to be hydrated. On the other hand, since the density of supercritical water near the critical point is so low that intermolecular water–water interactions are weakened, hydrophobic non-polar substances can be mixed with the gas-like low density water better than with condensed water in which strong water–water hydrogen-bonding interactions exist. However, it is obvious that supercritical water can have a wide density range and at very high pressure and high temperature, far above the critical point, supercritical water can have a density of 0.8–1.0 g cm^{-3} (as ambient water has) and we have an extremely limited amount of knowledge of the structure of supercritical water over such a wide range of densities.

The aim of the present article is to review recent results reported by using X-ray and neutron diffraction methods, IR and Raman spectroscopies and computer simulations for the structure and properties of supercritical water over a relatively wide range of density. Unfortunately, not many reports have appeared of NMR spectra, probably due to experimental difficulties.

2 Solution X-ray diffraction on sub- and super-critical water

X-Ray diffraction studies of liquids and solutions at HTHP have lagged behind those under ambient conditions, because of various technical difficulties: weak scattering from the small sample volume of an HTHP cell, elimination of strong Bragg reflections from the crystalline cell, a narrow measurable range due to geometrical constraints of the cell, *etc.* Great progress in X-ray diffraction at HTHP has been made, however, when intense X-rays became available in synchrotron radiation facilities world-wide. The most frequently used method there is the energy-dispersive diffraction with a multi-anvil cell made of boron nitride or a diamond anvil cell, with which pressures of 10 GPa, and temperatures of 1000 °C are available, and the maximum scattering variable given by eqn. (1)

$$s = 4\pi\lambda^{-1}\sin\theta \qquad (1)$$

(λ the wavelength and 2θ the scattering angle) of 0.10 pm^{-1} has been attained. These sample environments are appropriate for liquids containing heavy metals, but not useful for liquids of light elements like water, since the X-ray scattering intensity from a small volume of sample is too weak to analyse with a good confidence level.

In some laboratories, the energy-dispersive X-ray diffraction experiments for sub- and super-critical water were successfully made in a beryllium cell using a table-top type X-ray diffractometer equipped with a rotatory anode, at 500 °C and a pressure of 700 MPa being possible.[15,16] However, the energy-dispersive method has the inherent disadvantage of complication in data correction, which can be much simplified in the angle-dispersive mode, and only a limited scattering range is measurable at one time, although it does have the advantage of time saving by using a solid state detector (SSD). In order to overcome the above problems, a solution X-ray diffraction method for the angle-dispersive mode has recently been developed on a laboratory scale by using a two-dimensional imaging-plate (IP) detector.[22]

Figs. 1(*a*) and (*b*) show two types of X-ray diffractometers with an SSD[22] and an IP detector,[23] respectively, which have been used for X-ray scattering measurements of water at HTHPs. In both cases a similar HTHP sample environment [Fig. 1(*c*)] was employed with a spindle-shaped beryllium cell; the part through which the X-ray beam passed had a cylindrical form with a 6 mm outer diameter and a 1.2–2.0 mm inner diameter filled with water. A Mo-Kα X-ray beam (λ 71.07 pm) was employed. The diffraction ranges of $1° < \theta < 120°$ by the SSD detector and $0° < \theta < 144°$ by the IP detector were covered in each measurement. The high pressure unit was guaranteed by the makers up to 1 GPa. The pressure resistance of the cell was checked and calibrated up to 800 MPa with an uncertainty of 0.05 MPa. The high-temperature and high-pressure sample assembly was mounted in a vertical[23] or horizontal[22,24] manner on a high pressure support unit placed at the centre of the X-ray goniometers.

The structure function $sH(s)$ was derived from the observed intensities $I(s)$ and is usually defined by eqn. (2).

$$sH(s) = s\{[I_{corr}(s) - f^2(s)]/f^2(s)\}\exp(-bs^2) \qquad (2)$$

where $f(s)$ is the scattering factor for one water molecule, b is an arbitrary damping factor, and $I_{corr}(s)$ is the corrected and normalized intensity function. The pair correlation function $g(r)$ was derived from the structure function $sH(s)$ by the Fourier transform according to eqn. (3).

$$g(r) = 1 + (1/2\pi^2\rho_0)\int_0^\infty s^2 H(s)[\sin(sr)/sr]\mathrm{d}s \qquad (3)$$

where ρ_0 is the average number density of the molecules, and equal to 3.34×10^{-8} pm^{-3} at ambient temperature and pressure. The pair correlation function represents the possibility of the existence of atom pairs with definite separations, and

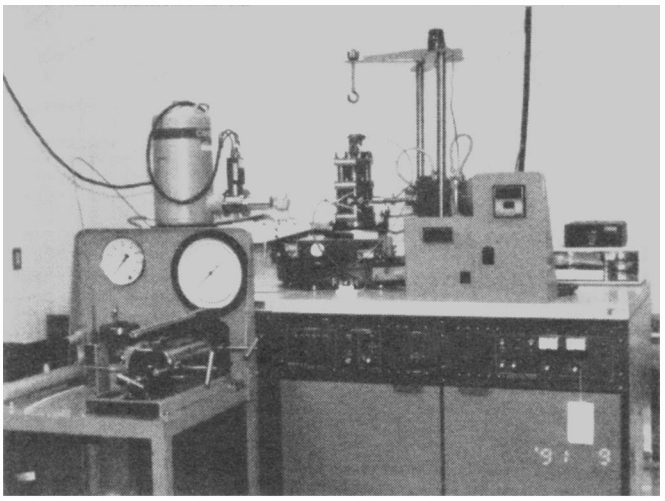

(a)

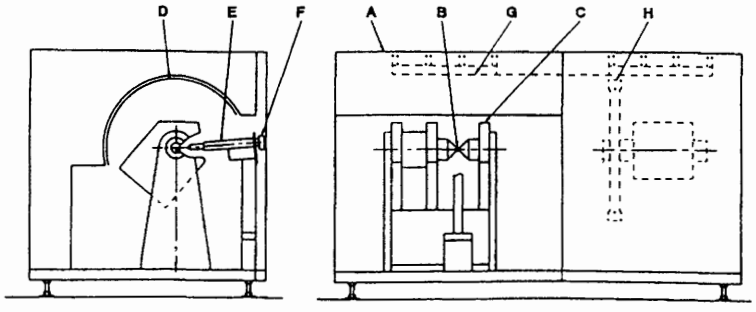

(b)

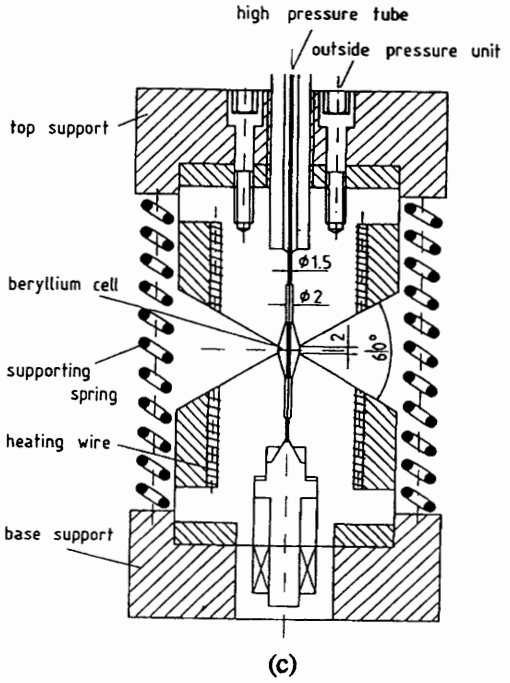

(c)

Fig. 1 High temperature-high pressure X-ray diffractometers. (*a*) A horizontal type diffractometer with an SSD detector. (*b*) A vertical type diffractometer with an imaging plate detector. A: diffractometer, B: beryllium cell, C: cell holder, D: slit, E: collimator, F: shield, G: imaging plate, H: imaging plate reader. (*c*) High temperature-high pressure cell and the holder. Quoted in refs. 23 and 24.

$g(r) = 1$ means that all atoms are distributed randomly so that no atom–atom pair correlation exists.

Structural parameters were obtained by a least-squares fitting procedure to minimize the difference χ^2 between experimentally obtained structure function $sH(s)$ and that from the model $sH_m(s)$ [eqns. (4) and (5)]:

$$\chi^2 = \sum_s [sH(s) - sH_m(s)]^2 = \min \quad (4)$$

$$H_m(s) = \rho_0 N[\sin(rs)/rs] \exp(-l^2s^2/2) \quad (5)$$

The sum in eqn. (4) was extended over each discrete s value in the measured range. The adjustable parameters of the model function were the distance between nearest neighbouring molecules r, coordination number N, and the parameter characteristic of the width of the main peak (temperature factor) l. Uncertainties in the values of r, N and l are usually 1–2 pm, 0.1–0.2, and ± 1–5 pm, depending on the accuracy of measurements, the shape of the peaks, *etc.*

An alternative definition for the coordination number may be given by computing the integral in eqn. (6):

$$N = 4\pi r^2 \rho_0 \int_0^r g(r)dr \quad (6)$$

where the upper limit of the integral is extended to the first minimum r_{min} of the $g(r)$ functions. There are various definitions for the upper limit of the integration, r, in the estimation of N. Diffraction researchers usually adopt the Gaussian distribution of atom pairs, and thus, the r value is the value of the upper tail of the Gaussian distribution (definition 1). On the other hand, simulation researchers usually take the r value as the point where the $g(r)$ function passes $g(r) = 1$ after the first maximum (definition 2). Some researchers define the integral limit at the value where the $g(r)$ function reaches the first minimum (definition 3), but this definition is not clear when the $g(r)$ function has a very shallow minimum. Of course, depending on the definitions the value of N changes. This definition of the coordination number in terms of the population of atoms until the r value at $g(r) = 1$ after the first maximum of $g(r)$ (definition 3) is favourable when we compare the coordination number obtained by the diffraction method and that by computer simulations. The coordination number evaluated by using definition 3 is sometimes called N_{min}.

3 Water structure at sub- and super-critical states

Thermodynamic data for water at the critical point are given as follows: the critical temperature T_c, 647.29 K (t_c = 374.14 °C); the critical pressure p_c, 22.064 MPa; the critical density ρ_c, 0.322778 g cm^{-3}.[25] It should be noted that the critical density is approximately one third of the density of normal water, and thus, when we discuss the water structure at HTHP near the critical point, we should pay careful attention to the density of water samples. In the present paper, we divide water into three categories: (*a*) low density water; $\rho < \rho_c$, (*b*) medium density water; $\rho_c \leqslant \rho < 1$ g cm^{-3}, and (*c*) high density water, 1 g cm^{-3} $\leqslant \rho$ (Fig. 2). Discussion concerning the low density water will not be included in the present paper.

In the high density region of water, in 1985 Gaballa and Neilson[17] performed the first angle-dispersive X-ray measurements on light and heavy water at room temperature over a pressure range from 0.1 to 600 MPa; the densities change from 0.997 g cm^{-3} at 0.1 MPa to 1.149 g cm^{-3} at 500 MPa for light water and from 1.104 g cm^{-3} at 0.1 MPa to 1.301 g cm^{-3} at 600 MPa for heavy water. They observed that with increasing pressure the first neighbour O–O peak at 290 pm in the radial distribution functions shifts to the shorter distance side and is enhanced, while the broad peaks at 440 and 700 pm ascribed to the second and third neighbour O–O interactions, respectively, shift to the shorter distance side and are decreased for both

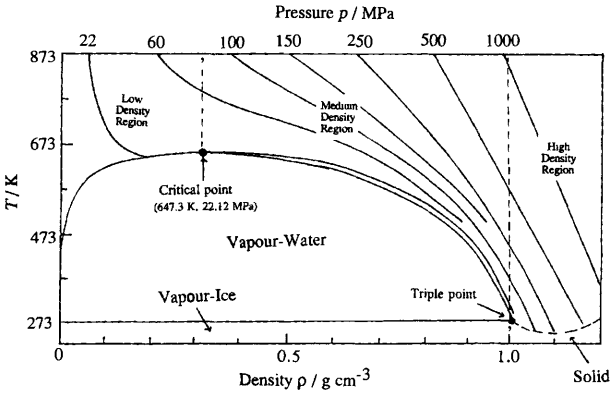

Fig. 2 Phase diagram of water around the critical point. A conventional classification of the high, medium, and low density regions is shown in the diagram. Quoted in ref. 32.

isotopic forms of water. These findings suggest the weakening of tetrahedral ordering in water as a result of compression, however, it should be noted that the peaks at 290, 440 and 650 pm are still clearly observed even at 600 MPa, suggesting that the tetrahedral ice-like structure remains at the high pressures. They analysed the first peak at 290 pm by a least-squares fitting procedure using a single Gaussian and found that the peak position shifts from 289 pm at 0.1 MPa to 284 pm at 500–600 MPa for both light and heavy water. The rate of contraction of the O–O separation was estimated to be *ca.* 100 pm GPa^{-1} (0.1 Å kbar^{-1}). The nearest neighbour O–O coordination number was found to increase from 4.4 at 0.1 MPa to *ca.* 4.9 at high pressure.

More recently, Gorbaty and his coworkers[18] published the results of energy-dispersive X-ray measurements of normal water at room temperature over a pressure range from 0.1 to 770 MPa. The pressure dependent features in the radial distribution functions obtained with this technique are broadly consistent with those obtained with the angle-dispersive technique by Gaballa and Neilson, but there are appreciable differences in the radial distribution functions obtained by the two different methods; a distinct shoulder appeared at *ca.* 320 pm, which has not been observed in the angle-dispersive data, and at *ca.* 600 MPa the 430 pm peak due to the second O–O interactions, clearly seen in the Gaballa–Neilson data, is almost invisible. They employed a least-squares fitting procedure with three Gaussians to resolve the first peak at 290 pm, a shoulder at *ca.* 320 pm, and the background at the longer distance. The first-neighbour O–O distance thus obtained showed a peculiar behaviour with pressure; when the pressure was raised from 0.1 to 200 MPa, the O–O distance decreased from 282 to 279 pm, but then gradually increases up to 282 at *ca.* 400 MPa and was almost constant at higher pressures. This result is not consistent with that obtained by Gaballa and Neilson. Since the paper does not show detailed numerical results of the radial distribution functions, we cannot discuss their results in more detail. However, it is difficult to understand such a peculiar change in the O–O distance, which may be caused by the peak separation procedure as was noted in the paper. The above inconsistencies in the structure of the high-density water at HTHPs between the two different methods have been discussed by Radnai and Ohtaki,[23] who have recently made angle-dispersive X-ray scattering experiments using SSD [Fig. 1(*a*)] on water in the medium-density to high-density region (d = 0.896–1.072 g cm^{-3}) over temperature and pressure ranges of 295–473 K and 0.1–200 MPa, respectively. The radial distribution curves obtained in this work are shown in Fig. 3. The structural parameters finally obtained are summarized in Table 1. The structural data at the different temperatures under vapour pressure agree well with the literature values measured at 298 K and 0.1 MPa (r = 287 pm and N = 3.33 and r = 285 pm and N = 3.53), at 373 K under vapour pressure (r = 291 pm and

N = 3.33), and 473 K under vapour pressure (r = 297 pm and N = 3.03). The structural parameters obtained under normal conditions are also in good agreement with the values obtained in previous X-ray diffraction measurements under similar experimental conditions.[15–18,26] As can be seen in Fig. 3, the broad peaks centred at 450 and 600 pm diminish with the increase in temperature, but they did not significantly change with pressure. The results indicate that temperature mainly affects both medium- and long-range ordering in the hydrogen-bonding network of water investigated, as has been discussed by many authors. The variation of the first peak at 285 pm with temperature and pressure gives us information about the effect of temperature and pressure on the hydrogen bonding in water. This topic will be discussed below.

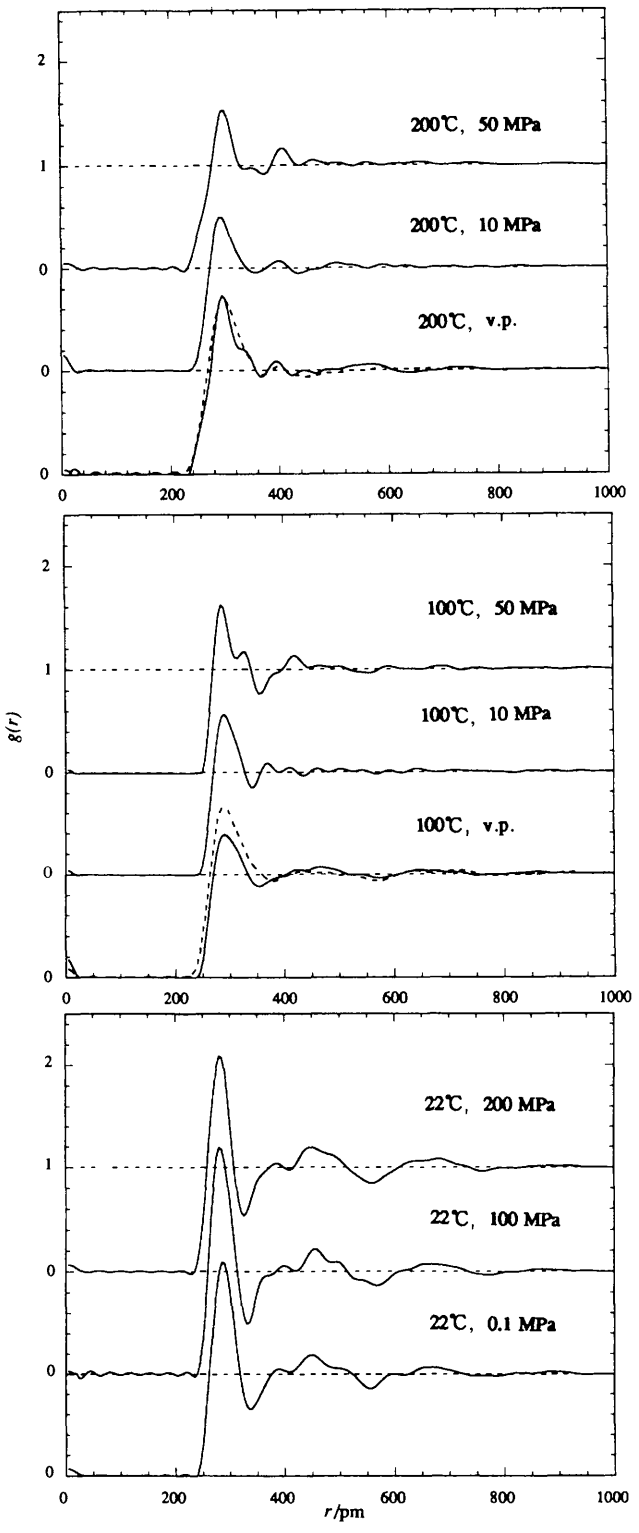

Fig. 3 Pair correlation functions $g(r)$ of water at various temperatures and pressures. Dashed lines represent data obtained by Narten and Levy.[26] Quoted in Ref. 23.

Table 1 Structural parameters of water at 295–485 K and 0.1–200 MPa (quoted in ref. 23)

T/K (t/°C)	p/MPa	ρ/g cm^{-3}[a]	r/pm	r_{min}/pm[b]	N
295 (2_2)	0.1	0.998	286	343	3.4
295 (2_2)	100	1.038	283	332	3.7
295 (2_2)	200	1.072	282	326	4.0
373 (100)	V.p.[c]	0.958	292	355	2.5
373 (100)	10	0.963	290	343	2.5
373 (100)	50	0.980	288	358	2.0
473 (200)	V.p.[c]	0.864	297	368	2.7
473 (200)	10	0.872	296	358	2.2
473 (200)	50	0.896	284[d]	375	2.2[d]

[a] Densities are quoted from the literature. [b] r_{min} denotes the r-value at the first minimum after the first main peak in the radial distribution curve. [c] V.p. indicates that the water is equilibrted with the vapour pressure under the given conditions. [d] Corrected values of those in ref. 23, unpublished data.

In the medium-density range of water and supercritical water, Gorbaty and Demianets published the first results of energy-dispersive X-ray diffraction of water over a temperature range of 298–773 K at a constant pressure of 100 MPa, with densities 1.1–0.7 g cm^{-3}.[15,16] The second peak at 450 pm in the radial distribution function, which provides strong evidence for tetrahedral ordering in water, diminishes gradually and is not observed at the subcritical temperature of 623 K. These findings show that the ice-like short-range order does not exist above this temperature. Furthermore, the peaks at 450 and 700 pm merge into one peak at *ca.* 600 pm. The position of the first peak changes linearly from 280 pm at 298 K to 304 pm at 773 K. They pointed out that the value of 304 pm at 773 K is shorter than the nearest-neighbour distance of 311 pm in liquid neon at the same reduced temperature,[27] indicating the presence of hydrogen bonds even at the highest temperature. They resolved the first peak into three Gaussians, *i.e.* the peaks at *ca.* 290 and 330 pm and the background. On the basis of the X-ray data together with IR spectral data, they calculated a parameter $x = a_1r_1/(a_1r_1 + a_2r_2)$, as an estimation of the fraction of hydrogen bonds in water,[27] where r_1 and r_2 are 290 and 330 pm, respectively, and the a_1 and a_2 are their peak areas. The x value changed linearly from 0.55 at room temperature to 0.2 at 773 K and was expressed by the empirical equation $x = (-8.68\ 10^{-4})T + 0.851$ with the absolute temperature T. According to this equation, it would be expected that the hydrogen bonds persist to *ca.* 30% at the critical temperature.

Recently, Yamaguchi and his group[24] reported a result on the water structure at HTHPs including a supercritical region over temperature and pressure ranges of 300–649 K and 0.1–98.1 MPa, respectively, using an HTHP X-ray diffractometer combined with an IP detector[22] [Fig. 1(*b*)].

They examined the water structure at constant densities from 1–0.7 g cm^{-3} with varying both temperatures and pressures. The measurement has the advantage in investigating the structure change in water with temperature and pressure without significant modification of the nearest-neighbour O–O distances by density variation. The radial distribution function is defined as eqn. (7).

$$D(r) - 4\pi r^2\rho_0 = (2r/\pi)\int_0^{S_{max}} si(s)M(s)\sin sr\ ds \qquad (7)$$

where

$$i(s) = K\, I_{obs}(s) - \sum_j n_j\{[f_j(s) + \Delta f_j'(s)]^2 + [\Delta f_j''(s)]^2 + \Phi(s)\, I_j^{inco}(s)\} \quad (8)$$

and

$$i_{calc}(s) = \sum_x \sum_y n_{xy} f_x(s) f_y(s)[\sin(r_{xy}s)/(r_{xy}s)]e^{-b_{xy}s^2} \quad (9)$$

Here, ρ_0 denotes the average scattering (electron) density of water, and $M(s) = [f^2(0)/f^2(s)]\exp(-0.01s^2)$. K is a constant to convert the scattering intensities $I_{obs}(s)$ to the absolute electron unit, n_j the number of atoms j in a unit volume, x and y the atom pair of x and y, $f_j(s)$ the scattering factor of atom j at s, $\Delta f_j'(s)$ and $\Delta f_j''(s)$ the real and imaginary parts of the anomalous dispersion term, $\Phi(s)$ the degree of incoherent scattering intensities $I_j^{inco}(s)$ reached the counter by atom j at s, n_{xy} the frequency factor or the coordination number of atom x around atom y, r_{xy} the distance between atoms x and y, b_{xy} the temperature factor of the atom pair x and y, which relates to the mean square amplitude $<l^2>$ through the relation $b_{xy} = <l_{xy}^2>/2$. n_{xy}, r_{xy}, and b_{xy} are the values to be determined. The radial distribution curves obtained by the X-ray diffraction method by using an IP detector at various temperatures and pressures[24] are shown in Fig. 4.

As is seen in Fig. 4, the peaks at 450 and 670 pm are not observed at 416 K when the pressure of 52.9 MPa is applied,

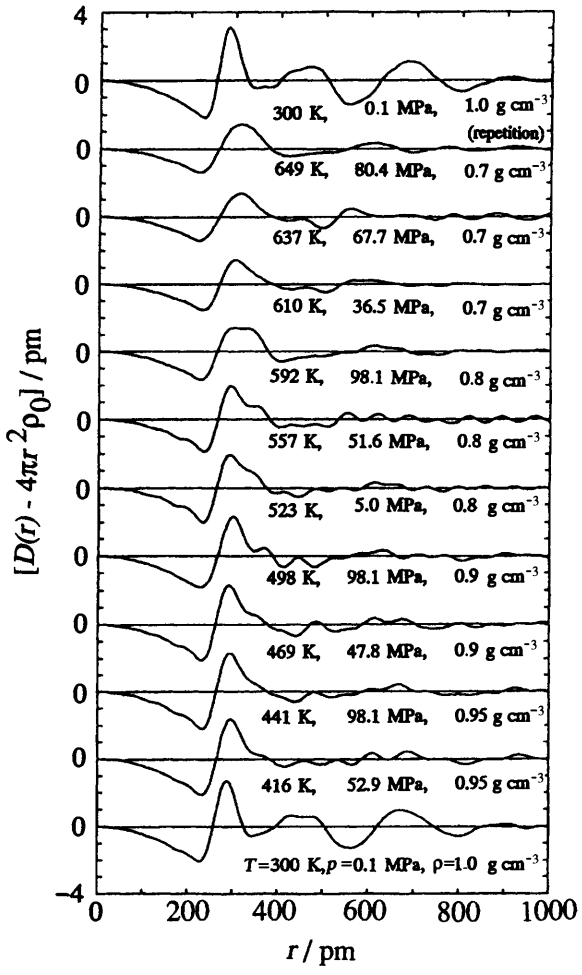

Fig. 4 The radial distribution curves of high temperature and high pressure water. The radial distribution curve of the normal water is given to show the reproducibility of the measurement and is shown as the reference. Quoted in ref. 24.

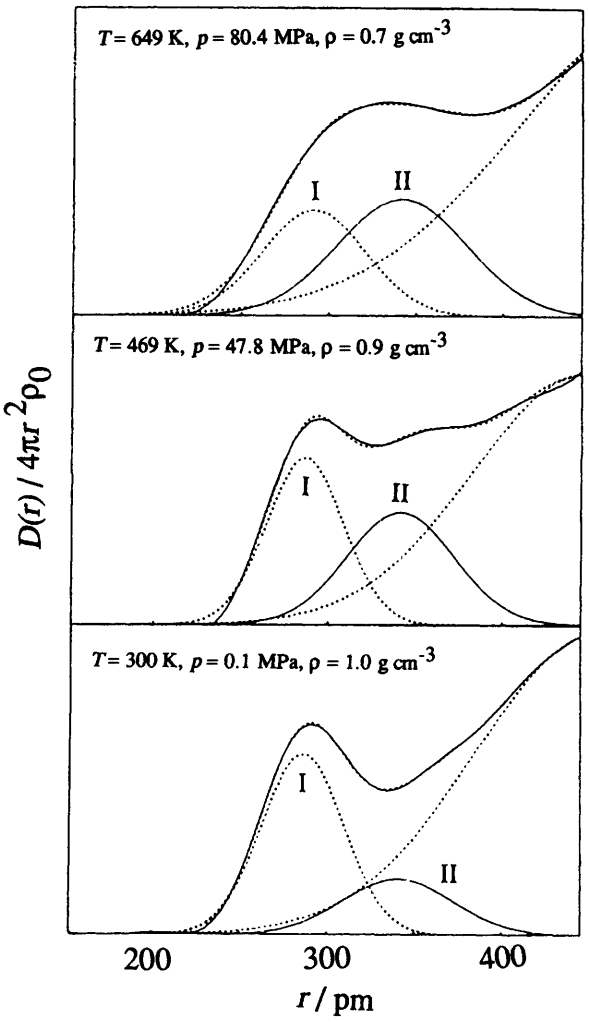

Fig. 5 Examples of the peak analysis of radial distribution functions $D(r)/4\pi r^2\rho_0$. The experimental values are given by solid lines and the calculated ones by dots. I and II indicate the H-bonded and the non-H-bonded nearest neighbour water molecules. Quoted in Ref. 24.

showing the loss of the tetrahedral ice-like ordering of water. A typical trend of the radial distribution functions with increasing pressure and temperature is that the first peak gradually broadens and shifts to the longer distance and the second peak at 450 pm and the third one at 670 pm merge into one peak at *ca.* 600 pm. These features are in qualitative agreement with the energy-dispersive data of Gorbaty, *et al.* At a supercritical temperature of 649 K with a medium density (ρ *ca.* 0.7 g cm^{-3}), the feature of radial distribution function is very similar to that for liquid mercury at low density (*ca.* 10 g cm^{-3}), suggesting that the overall structure of the medium density supercritical water resembles that of simple liquids except for hydrogen bonding with the nearest neighbours.

The first peak of the radial distribution curves was resolved into two peaks I and II (Fig. 5), as carried out by Gorbaty, *et al.* The former had a peak position of 287–292 pm and was ascribed to the O–O distance of contacted water molecules. The position of the latter peak appeared at *ca.* 340–348 pm and it may be attributable to non-bonding water–water distances in water. The O–O distances r found from the position of the peaks I and II, the coordination numbers N calculated from the peak area, and the half-width of half-height of the peaks σ are given in Table 2 and are also plotted in Fig. 6. The sum of the two N values, $N = N_I + N_{II}$, is also shown in Fig. 6. The intermolecular O–O distances for peaks I and II do not change significantly over the temperature range investigated as expected from the constant density measurement. On the contrary, with increasing tem-

perature N_I decreases from 3.1 at 300 K to 1.6 at a supercritical temperature of 649 K, whereas N_{II} increases from 1.3 to 2.3; the sum, N, remains practically constant at *ca.* 4, although a slight decrease in N may be seen with a decrease in the density. These results show that the hydrogen bonds are gradually broken and/or distorted with increasing temperature, but the degree of the hydrogen bond formation still remains *ca.* 40% above the critical point. Another interesting finding is that the values of σ for peaks I and II are almost constant at $\leqslant$604 K but increase when the temperature approaches the critical point. This finding indicates that the nearest-neighbour O–O bonds fluctuate largely around the critical temperature.

If we assume that the liquid phase homogeneously expands and is compressed by the change of temperature and pressure, the distance between the adjacent water molecules should be proportional to $\rho^{-1/3}$, eqn. (10):

$$r = k\, r_0\, \rho^{-1/3} \qquad (10)$$

where r_0 denotes the O–O distance in the reference state, water under an ambient condition in this case. k is a proportionality constant and should be unity if we assume a homogeneous variation of the volume of water with temperature and pressure. The r values in Table 1[22] and the r_I values in Table 2[23] are plotted against $\rho^{-1/3}$ in Fig. 7. We can see from Fig. 7 that the O–O distance changes almost linearly with $\rho^{-1/3}$ over a limited range of the density change from 0.95–1.04 g cm^{-3}, but in the lower ($\geqslant$0.92 g cm^{-3}) density region, the change in the O–O distance deviates from the straight line given by eqn. (10), although the deviation of the O–O distance in the higher (1.072 g cm^{-3}) density region is unclear. It is obvious that in the lower density region, the O–O distance cannot be elongated to produce the given densities.

A plot of the coordination number, N, vs. density, ρ, is given in Fig. 8. The coordination number increases monotonically with increasing density, and we do not see a particular irregularity in the variation of N with ρ. Thus, we can conclude that over the temperature and pressure ranges examined, expansion and compression of water by changing temperature and pressure have a more direct effect in changing the coordination number than the O–O distance. From the observations in the changes in the O–O distance, coordination number, and the temperature factors with density at HTHPs, we can draw the following conclusions:

(1) Most hydrogen-bonding in water is weakened and/or decomposed at elevated temperatures and pressures, but some water molecules associate to form a condensed phase with short O–O distances under sub- and super-critical conditions.

(2) Since the coordination number decreases with a decrease in density and the O–O distance does not change in proportion to the change in $\rho^{-1/3}$, the condensed water phase cannot expand homogeneously over the whole space, and thus, under supercritical conditions water molecules may form clusters containing a relatively small number of water molecules with a limited O–O separation of 280–295 pm.

(3) The clusters may be spread over the whole space of supercritical water, and there may be smaller aggregates than clusters with a small number of water molecules—oligomers to monomer—to construct a very diffuse phase of water.

(4) Since the coordination number decreases rather quickly with density, the size of the clusters may not be so large, because water molecules at the surface of the clusters, which should have a smaller coordination number than those in the core, should contribute significantly to the decrease in N with ρ.

(5) Water molecules in the core of the clusters and aggregates are surrounded by a relatively small number of water molecules at HTHPs due to decomposition of hydrogen bonds, while the number of non-hydrogen-bonded water molecules increases with increasing pressure or density due to compression of the volume of water with pressure.

(6) Therefore, it is most likely that water at HTHPs consists of a mixture of clusters containing a relatively small number of water molecules and much smaller aggregates such as oligomers and even monomers of water molecules.

4 Comparison of the views derived from the X-ray diffraction measurements and other studies

Pair correlation functions of sub- and super-critical water obtained by various experiments and computer simulations are summarized in Fig. 9. Since they have different weights for different atom pairs, the shape of the curves are, of course, not the same, but we can see a qualitative picture of the structure of water under such conditions from the peak shapes and peak positions. More detailed discussion should be done by analysing the curves using eqn. (9) for the results of X-ray diffraction measurements and their equivalents for other studies.

Neutron diffraction measurements have been made on three different types of isotopically enriched water under subcritical (423 and 573 K, 10–280 MPa, 0.72–1.0 g cm^{-3}) and supercritical (673 K, 80 MPa, 0.66 g cm^{-3}) conditions, from which three partial pair correlation functions, $g_{OH}(r)$, $g_{HH}(r)$, and $g_{OO}(r)$ have been determined.[21] Although the contribution of O–O pairs to the total intensities is small (*ca.* 10%), the pair correlation function $g_{OO}(r)$ obtained at 673 K is compared with those obtained from other techniques [see Fig. 9(*e*)]. $g^{ND}(r)$ (the superscript ND denotes the data obtained from a neutron diffraction study) and shows a large shoulder at *ca.* 230 pm, which has not been found in the X-ray diffraction study[24] [Fig. 9(*f*)]. The peak at *ca.* 280 pm is sharper in the $g^{ND}(r)$ function than in $g^{XD}(r)$ (XD means X-ray diffraction).[24] A broad peak at *ca.* 500–700 pm appears in both curves, although the former shows it more clearly than the latter.

Results from computer simulations for supercritical water give good suggestions for interpretation of diffraction data. Many attempts have been carried out for the structure of supercritical water using various types of pair potentials such as TIP4P,[10,11] SPC,[12,28] SPCE,[13] and SPCG.[29] The pair correla-

Table 2 Structural parameters of medium density water. Quoted in ref. 24

			Peak I			Peak II		
T/K (t/°C)	p/MPa	ρ/g cm^{-3}	r_I/pm	N_I	σ_I/pm	r_{II}/pm	N_{II}	σ_{II}/pm
300 (27)	0.1	1.0	287	3.1	0.28	341	1.3	0.37
416 (143)	52.9	0.95	291	2.8	0.27	341	1.8	0.34
441 (168)	98.1	0.95	290	2.8	0.27	340	1.9	0.32
469 (196)	47.8	0.9	287	2.5	0.26	342	2.4	0.36
498 (225)	98.1	0.9	290	2.4	0.27	342	2.4	0.36
523 (250)	5.0	0.8	287	2.1	0.26	339	2.2	0.34
557 (284)	51.6	0.8	289	2.1	0.25	344	2.1	0.35
592 (319)	98.1	0.8	287	2.1	0.30	343	2.4	0.34
610 (337)	36.5	0.7	293	1.8	0.31	348	1.9	0.42
637 (364)	67.7	0.7	293	1.7	0.33	343	2.0	0.42
649 (376)	80.4	0.7	292	1.6	0.35	342	2.3	0.44

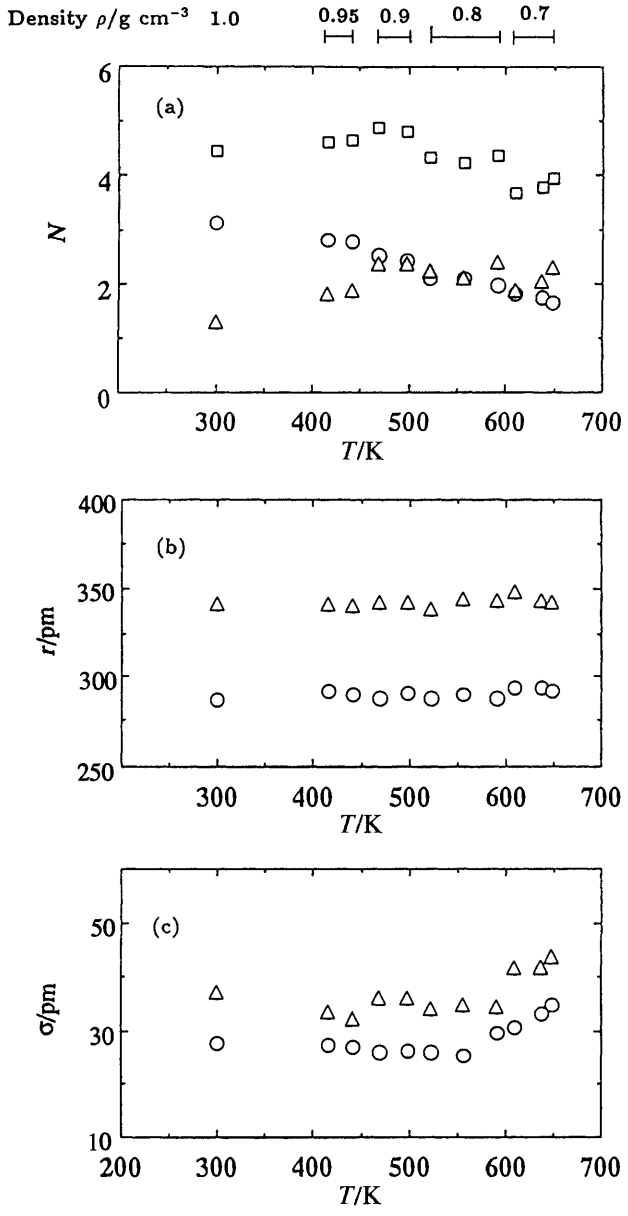

Fig. 6 The results of peak analysis of the radial distribution functions shown in Fig. 4. (*a*) Coordination numbers of peaks I and II and their sum, (*b*) their interatomic distances, and (*c*) their full-width at half height against the temperature. Quoted in ref. 24.

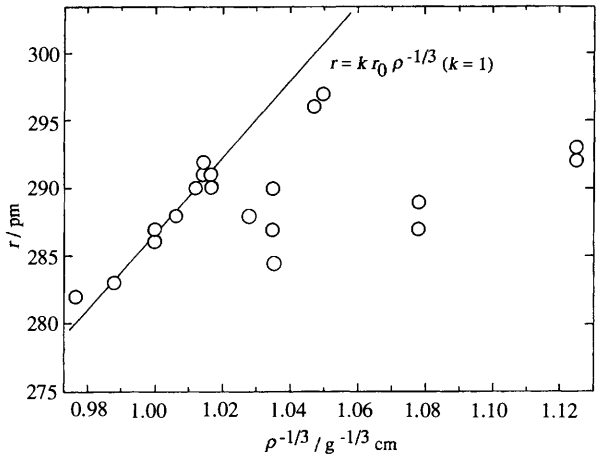

Fig. 7 Variation of the O–O distance (r) in water as a function of $\rho^{-1/3}$. The solid line represents the change in r calculated by assuming a homogeneous expansion of water with ρ. The line given by $r = k\, r_0 \rho^{-1/3}$ at $k = 1$.

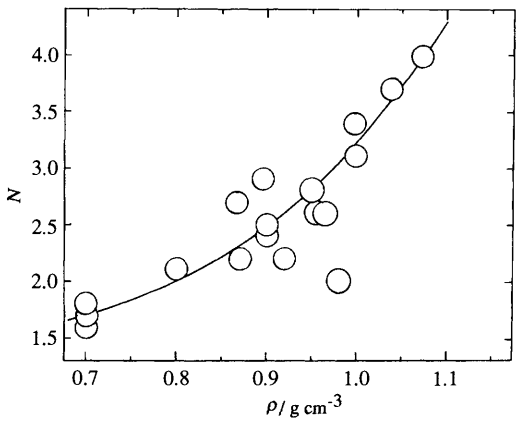

Fig. 8 The variation of the coordination number N with density ρ

tion functions, $g(r)$, obtained with these simulations and diffraction methods are also summarized in Fig. 9. The shape of the curves is similar in all cases, except for $g^{ND}(r)$ [Fig. 9(*e*)], and the first peak at *ca.* 280 pm in all $g^{CS}(r)$ (CS denotes the function calculated from computer simulation) is sharper than that in $g^{XD}(r)$. Since the density of supercritical water examined by the SPCE model[13] (0.33 g cm^{-3}) is much lower than that used for the neutron[21] (0.66 g cm^{-3}) and X-ray[23,24] (0.7–0.9 g cm^{-3}) diffraction experiments, a direct comparison between $g^{CS}(r)$ and $g^{ND}(r)$ or $g^{XD}(r)$ may be difficult. Results obtained by using the TIP4P model [Figs. 9(*a*) and (*b*)] should be similar to those obtained by diffraction methods, because the densities of the examined water are rather similar. However, a remarkable difference is seen in $g^{ND}(r)$ from the other $g(r)$ values for the shoulder at *ca.* 230 pm and a deep valley appearing at *ca.* 420 pm. A further, careful investigation may be needed for neutron diffraction experiments, since the valley appearing in the $g^{XD}(r)$ curves under subcritical conditions [Fig. 9(*g*)] becomes shallow as temperature and pressure increase and no marked valley appears in $g^{XD}(r)$ and $g^{CS}(r)$ of supercritical water; the deep valley in $g^{ND}(r)$ may be a spurious one, as the shoulder at *ca.* 230 pm in $g^{ND}(r)$.

SPC (μ = 7.586 10^{-30} C m, where μ denotes the dipole moment of a water molecule) and SPCE (μ = 7.843 10^{-30} C m) water molecules have dipole moments larger by 23 and 27%, respectively, than that of an isolated water molecule (μ = 6.187 × 10^{-30} C m). The dipole moment of the SPCG water molecule is the same as that of an isolated water molecule. Therefore, we can expect that hydrogen-bonding interactions and dipole–dipole electrostatic interactions are weaker in the SPCG water than in SPC and SPCE waters. In fact, the $g_{OH}(r)$ curve obtained by using the SPCE model has larger peaks at *ca.* 180 and 320 pm, the former should correspond to the distance between a hydrogen atom of the central water molecule and the oxygen molecule in the adjacent water molecule and the latter indicates the O···H separation between the central water molecule and the hydrogen atom in the adjacent water molecule.[28] However, the neutron diffraction experiment[21] did not show the peak at *ca.* 180 pm (Fig. 10). Probably more careful neutron diffraction experiments should be repeated. On the other hand, more sophisticated pair potentials for supercritical water should be developed toward recent attempts to take into account the effect of polarizability of water and the many-body effect.

Diffraction experiments can provide the distribution of distances between atoms. However, the distance does not directly tell us whether they are bonding or not. Such

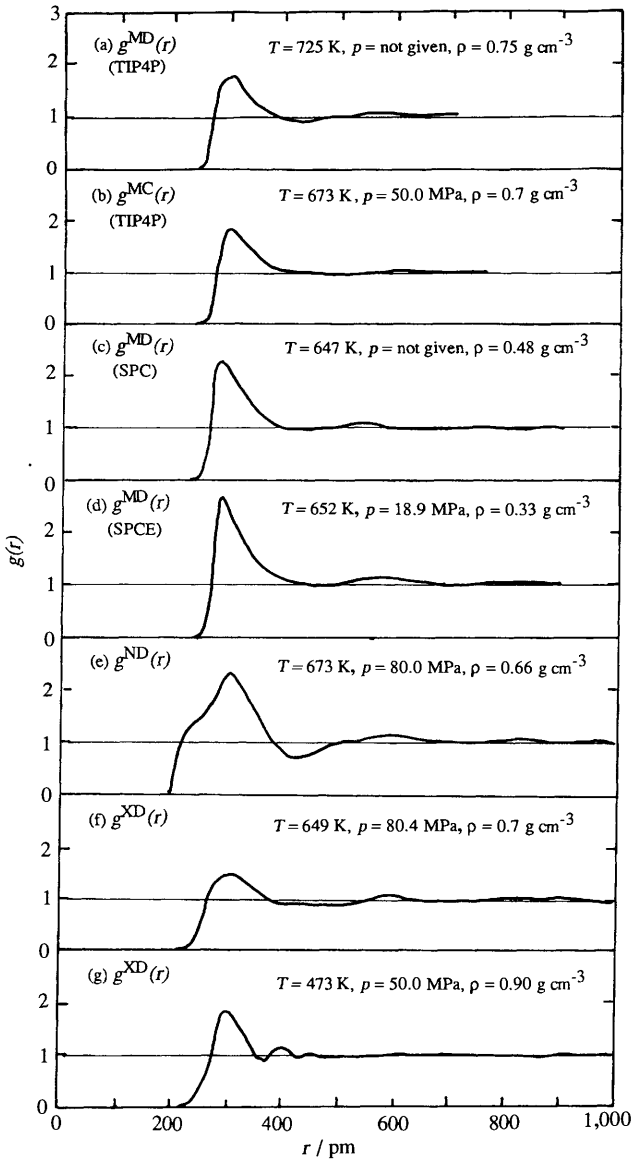

Fig. 9 Comparison of pair correlation functions $g(r)$ of various HTHP water samples examined by different methods. Superscripts MC and MD represent Monte Carlo and molecular dynamics simulations, respectively. ND and XD mean neutron and X-ray diffraction measurements, respectively. (*a*): ref. 10, (*b*): ref. 14, (*c*): ref. 12, (*d*): ref. 13, (*e*): ref. 21, (*f*): ref. 24, (*g*): ref. 23. Data in (*g*) were obtained under subcritical conditions. Quoted in ref. 31 except for (*g*).

information may be given by the value by comparing it with other experimental values which are known as the bond lengths. On the other hand, the frequency measurements by IR and Raman spectroscopies are more sensitive for the bonding nature, but usually they do not give us the value of the distance between atoms. Thus, both methods should be applied complementarily. The NMR method is especially useful for obtaining dynamic information of water molecules. However, application of high temperature and high pressure to the NMR cell is not easy and extremely limited attempts have been made by NMR specialists.

IR and Raman spectroscopic investigations for supercritical water were carried out much earlier than diffraction experiments and computer simulation. Franck and Roth[2] studied the O–D stretching frequency of HDO containing 8.5 mol% D_2O in H_2O at 303–673 K and 5–400 MPa (Fig. 11). A sharp band at 2719 cm^{-1} in HDO water having a density of 0.0165

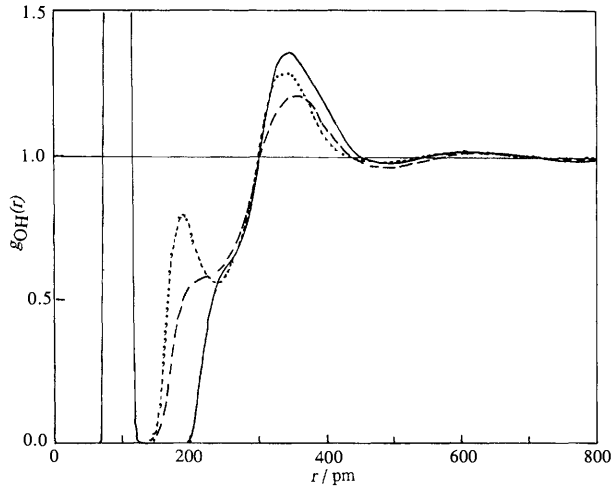

Fig. 10 Comparison among the partial pair correlation function $g_{OH}(r)$ obtained by computer simulations (dashed line: ref. 29) and a neutron diffraction experiment (solid line: ref. 21) for water at T = 673 K and ρ = 0.66 g cm^{-3}. Dots represent $g_{OH}(r)$ of water under the normal conditions. Quoted in ref. 33.

g cm^{-3} was not observed in water with a higher density than 0.095 g cm^{-3}. On the other hand, a broad band at 2650 cm^{-1} increased and shifted towards the lower wavenumber side with density, and in water with the density of 0.9 g cm^{-3} the band was observed as a big broad band centred at 2600 cm^{-1}. A more intense $\nu_{O\text{-}D}$ band was observed at 2520 cm^{-1} in water with the density of 1.0 g cm^{-3} at 303 K. The authors explained that a sharp band found at 2719 cm^{-1} in water with the density of 0.0165 g cm^{-3} at 673 K should correspond to the $\nu_{O\text{-}D}$ band without hydrogen bonding, while the broad and intense 2520 cm^{-1} band observed in the water should indicate that water molecules are hydrogen bonded.

Kohl, Lindner and Franck[6] employed Raman spectroscopy to a study of water with almost constant density of 0.8–1.0 g cm^{-3}. According to their results the broad O–D stretching band in HDO water appeared at *ca.* 2510 cm^{-1} at room temperature, which shifted towards the high frequency side and was sharpened with increased temperature. Under supercritical conditions at 673 K (the density of water was 0.04 g cm^{-3}) the band became very sharp and the band at 2510 cm^{-1} completely disappeared. The shape of the sharp band is close to that in the gas phase. From these results we may say that hydrogen-bonding interactions among water molecules still exist in supercritical water with a density greater than 0.1–0.2 g cm^{-3}.

Giguere[30] measured the O–H stretching band in water at high temperature and amorphous ice by Raman spectroscopy, and discussed two different O–H bonds, one having the normal O–H hydrogen-bonding distance of 185 pm and the other having 230 pm which resulted from a bifurcated O–H···O hydrogen bond. He explained that the former bond was formed predominantly at low temperatures and the contribution of the latter increased with increased temperature. The O–O distance may be kept practically unchanged with the change in temperature. His interpretation means that the tetrahedral ice-like water structure is practically unchanged, while the central water molecule rotates along the axis of one O-H···O hydrogen bond in the tetrahedrally coordinated water structure with temperature. However, it is difficult to say that hydrogen bonds are still formed in the bifurcated form, because the O-H···O angle in the bonded water molecules should be bent by more than 50°. Since the H···O distance at *ca.* 330 pm can still be detected in the neutron diffraction study[21] and computer simulations,[28] the interaction may be better attributed to the weak interaction between the hydrogen atom of the central water molecule and a second neighbour water molecule which approaches the central water molecule to *ca.* 330 pm.

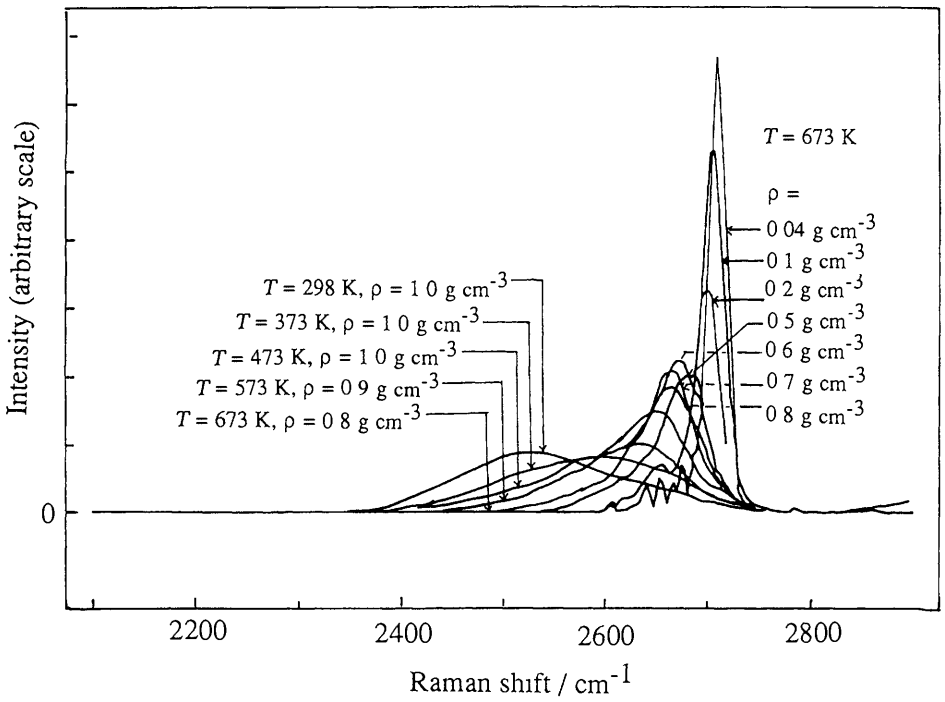

Fig. 11 Isotropic Raman spectra for the $\nu_{(D\ O)}$ stretching mode in 9 7 mol% HDO in H_2O at various temperatures and densities Quoted in ref 6

5 Concluding Remarks

Supercritical water has attracted scientists' interest in recent years due to its peculiar physicochemical properties and industrial uses. However, structural information on supercritical water is limited. The lack of structural information prevents the development of physicochemical studies of supercritical water because we do not have sufficient information for intermolecular interactions. We have reviewed recent investigations on the structure of sub- and super-critical water, and concluded, on the basis of structural data so far obtained, that water at HTHPs consists of a mixture of clusters and the dispersed phase contains low aggregates including monomeric water molecules. We predict extensive development of this field in the near future. Investigations of ionic solvation and complex formation reactions in supercritical water have begun in some laboratories.[32 33] Knowledge of hydration of ions and polar substances in supercritical water is important to understand ion–water and polar molecule–water interactions which relate to solubility phenomena and decomposition of the substances. The drastic change in the acid–base properties of water is also related to chemical relations of water with polar and non-polar molecules. Studies on the formation and decomposition reactions of organic substances in supercritical water may open another potentially useful field of chemistry. The expected development of chemistry in the 21st century will certainly necessitate a microscopic level exploration of supercritical water.

6 References

1 J D Bernal and R H Fowler, *J Chem Phys*, 1933, **1**, 515
2 E U Franck and K Roth, *Discuss Faraday Soc*, 1967, **43**, 108
3 C I Ratcliffe and D E Irish, *J Phys Chem*, 1982, **86**, 4897
4 N C Holms, W J Nellis, W B Graham and G E Walrafen, *Phys Rev Lett*, 1985, **55**, 2433
5 G E Walrafen, M S Hokmadadi, W -H Yang and G J Piermarini, *J Phys Chem*, 1988, **92**, 4540
6 W Kohl, H A Lindner and E U Franck, *Ber Bunsenges Phys Chem*, 1991, **95**, 1586
7 R W Impey, M L Klein and I R McDonald, *J Chem Phys*, 1981, **74**, 647
8 A G Kalinichev, *Int J Thermophys*, 1986, 7, 887
9 Y Kataoka, *J Chem Phys*, 1987, **87**, 589
10 R D Mountain, *J Chem Phys*, 1989, **90**, 1866
11 A G Kalinichev, *Z Naturforsch Teil A*, 1991, **46**, 433, 1992, **47**, 992
12 P T Cummings, H D Cochran, J M Simonson, R E Mesmer and S Karaborni, *J Chem Phys*, 1991, **94**, 5606
13 Y Guissani and B Guillot, *J Chem Phys*, 1993, **98**, 8221
14 A G Kalinichev and J D Bass, *Chem Phys Lett*, 1994, **231**, 301
15 Yu E Gorbaty and Yu N Demianets, *Z Strukt Khim*, 1983, **24**, 66
16 Yu E Gorbaty and Yu N Demianets, *Z Strukt Khim*, 1983, **24**, 74
17 G A Gaballa and G W Neilson, *Mol Phys*, 1983, **50**, 97
18 A V Okhulkov, Yu N Demianets and Yu E Gorbaty, *J Chem Phys*, 1994, **100**, 1578
19 T Yamaguchi, Y Tamura, H Ohtaki, S Ikeda and M Misawa, *KENS Report*, 1986, **6**, 125
20 K Ichikawa, Y Kameda, T Yamaguchi, H Wakita and M Misawa, *Mol Phys*, 1991, **73**, 79
21 P Postorino, R H Tromp, M -A Ricci, A K Soper and G W Neilson, *Nature*, 1993, **366**, 668, R H Tromp, P Postorino, G W Neilson, M A Ricci, and A K Soper, *J Chem Phys*, 1994, **101**, 6210, P Postorino, M A Ricci and A K Soper, *J Chem Phys*, 1994, **101**, 4123
22 M Ihara, T Yamaguchi, H Wakita and S Matsumoto, *Advances in X-ray Analysis (in Japanese)*, 1994, **25**, 49
23 T Radnai and H Ohtaki, *Mol Phys*, 1996, **87**, 103
24 K Yamanaka, T Yamaguchi and H Wakita, *J Chem Phys*, 1994, **101**, 9830
25 *IAPWS Release on the Skeleton Tables 1985 for the Thermodynamic Properties of Ordinary Water Substance*, 1994, *IAPWS Release on the Values of Temperature, Pressure, and Density of Ordinary and Heavy Water Substances at their Respective Critical Points*, 1992
26 A H Narten, M D Danford and H A Levy, *ORNL-3997*, 1966, *Disc Faraday Soc*, 1967, **43**, 97, A H Narten, *ORNL-4578*, 1970, A H Narten and H A Levy, *J Chem Phys*, 1971, **55**, 2263
27 Yu E Gorbaty and A G Kalinichev, *J Chem Phys*, 1995, **99**, 5336
28 J J Pablo, J M Prausnitz, H J Strauch and P T Cummings, *J Chem Phys*, 1990, **93**, 7355
29 A A Chialvo and P T Cummings, *J Chem Phys*, 1994, **101**, 466

30 P. A. Giguere, *J. Raman Spectrosc.*, 1984, **15**, 354; *J. Chem. Phys.*, 1987, **87**, 4835.
31 K. Yamanaka, H. Ozono, T. Yamaguchi and H. Wakita, *Progress in X-ray Analysis (in Japanese)*, 1995, **26**, 125.
32 E. U. Franck, *The Physics and Chemistry of Aqueous Ionic Solutions*, ed. M.-C. Bellissent-Funel and G. W. Neilson, Reidel, Dordrecht, p. 337, 1987.
33 T. Yamaguchi, M. Yamagami, H. Ohzono, H. Wakita and K. Yamanata, *Chem. Phys. Lett.*, 1996, **252**, 317.

Received, 2nd July 1996
Accepted, 17th October 1996